Open access • Journal Article • DOI:10.1088/0004-637X/774/1/68

Explaining the [CII]158um Deficit in Luminous Infrared Galaxies - First Results from a Herschel/PACS Study of the GOALS Sample

Tanio Díaz-Santos, Lee Armus, Vassilis Charmandaris, Vassilis Charmandaris ...+26 more authors

Institutions: California Institute of Technology, Institution of Engineers, Sri Lanka, University of Crete, University of Virginia ...+9 more institutions

Published on: 10 Jul 2013 - arXiv: Cosmology and Nongalactic Astrophysics

Topics: Luminous infrared galaxy

The Astrophysical Journal, 774:68 (13pp), 2013 September 1 doi:10.1088/0004-637X/774/1/68

EXPLAINING THE [C II]157.7 μm DEFICIT IN LUMINOUS INFRARED GALAXIES—FIRST RESULTS FROM A *HERSCHEL*/PACS STUDY OF THE GOALS SAMPLE

T. Díaz-Santos[1], L. Armus[1], V. Charmandaris[2,3,4], S. Stierwalt[5], E. J. Murphy[6], S. Haan[7], H. Inami[8], S. Malhotra[9], R. Meijerink[10], G. Stacey[11], A. O. Petric[12], A. S. Evans[5,13], S. Veilleux[14,15], P. P. van der Werf[16], S. Lord[17], N. Lu[12,18], J. H. Howell[1], P. Appleton[17], J. M. Mazzarella[5], J. A. Surace[1], C. K. Xu[17], B. Schulz[12,18], D. B. Sanders[19], C. Bridge[12], B. H. P. Chan[12], D. T. Frayer[20], K. Iwasawa[21], J. Melbourne[22], and E. Sturm[23]
[1] Spitzer Science Center, California Institute of Technology, MS 220-6, Pasadena, CA 91125, USA; tanio@ipac.caltech.edu
[2] IESL/Foundation for Research and Technology-Hellas, GR-71110, Heraklion, Greece
[3] Chercheur Associé, Observatoire de Paris, F-75014 Paris, France
[4] Department of Physics, University of Crete, GR-71003, Heraklion, Greece
[5] Department of Astronomy, University of Virginia, P.O. Box 400325, Charlottesville, VA 22904, USA
[6] Observatories of the Carnegie Institution for Science, 813 Santa Barbara Street, Pasadena, CA 91101, USA
[7] CSIRO Astronomy and Space Science, Marsfield NSW 2122, Australia
[8] National Optical Astronomy Observatory, 950 North Cherry Avenue, Tucson, AZ 85719, USA
[9] School of Earth and Space Exploration, Arizona State University, Tempe, AZ 85287, USA
[10] Kapteyn Astronomical Institute, University of Groningen, P.O. Box 800, NL-9700 AV Groningen, The Netherlands
[11] Department of Astronomy, Cornell University, Ithaca, NY 14853, USA
[12] Astronomy Department, California Institute of Technology, Pasadena, CA 91125, USA
[13] National Radio Astronomy Observatory, 520 Edgemont Road, Charlottesville, VA 22903, USA
[14] Joint Space-Science Institute, University of Maryland, College Park, MD 20742, USA
[15] Department of Astronomy, University of Maryland, College Park, MD 20742, USA
[16] Leiden Observatory, Leiden University, P.O. Box 9513, NL-2300 RA Leiden, The Netherlands
[17] NASA Herschel Science Center, IPAC, California Institute of Technology, MS 100-22, Cech, Pasadena, CA 91125, USA
[18] Infrared Processing and Analysis Center, MS 100-22, California Institute of Technology, Pasadena, CA 91125, USA
[19] Institute for Astronomy, University of Hawaii, 2680 Woodlawn Drive, Honolulu, HI 96822, USA
[20] National Radio Astronomy Observatory, P.O. Box 2, Green Bank, WV 24944, USA
[21] ICREA and Institut de Cincies del Cosmos (ICC), Universitat de Barcelona (IEEC-UB), Marti i Franques 1, E-08028 Barcelona, Spain
[22] Caltech Optical Observatories, Division of Physics, Mathematics and Astronomy, MS 301-17, California Institute of Technology, Pasadena, CA 91125, USA
[23] Max-Planck-Institut für extraterrestrische Physik, Postfach 1312, D-85741 Garching, Germany
Received 2013 February 15; accepted 2013 July 9; published 2013 August 19

ABSTRACT

We present the first results of a survey of the [C II]157.7 μm emission line in 241 luminous infrared galaxies (LIRGs) comprising the Great Observatories All-sky LIRG Survey (GOALS) sample, obtained with the PACS instrument on board the *Herschel Space Observatory*. The [C II] luminosities, $L_{[\mathrm{C\,II}]}$, of the LIRGs in GOALS range from $\sim 10^7$ to 2×10^9 $L_\odot$. We find that LIRGs show a tight correlation of [C II]/FIR with far-IR (FIR) flux density ratios, with a strong negative trend spanning from $\sim 10^{-2}$ to 10^{-4}, as the average temperature of dust increases. We find correlations between the [C II]/FIR ratio and the strength of the 9.7 μm silicate absorption feature as well as with the luminosity surface density of the mid-IR emitting region (Σ_{MIR}), suggesting that warmer, more compact starbursts have substantially smaller [C II]/FIR ratios. Pure star-forming LIRGs have a mean [C II]/FIR $\sim 4 \times 10^{-3}$, while galaxies with low polycyclic aromatic hydrocarbon (PAH) equivalent widths (EWs), indicative of the presence of active galactic nuclei (AGNs), span the full range in [C II]/FIR. However, we show that even when only pure star-forming galaxies are considered, the [C II]/FIR ratio still drops by an order of magnitude, from 10^{-2} to 10^{-3}, with Σ_{MIR} and Σ_{IR}, implying that the [C II]157.7 μm luminosity is not a good indicator of the star formation rate (SFR) for most local LIRGs, for it does not scale linearly with the warm dust emission most likely associated to the youngest stars. Moreover, even in LIRGs in which we detect an AGN in the mid-IR, the majority (2/3) of galaxies show [C II]/FIR $\geqslant 10^{-3}$ typical of high 6.2 μm PAH EW sources, suggesting that most AGNs do not contribute significantly to the FIR emission. We provide an empirical relation between the [C II]/FIR and the specific SFR for star-forming LIRGs. Finally, we present predictions for the starburst size based on the observed [C II] and FIR luminosities which should be useful for comparing with results from future surveys of high-redshift galaxies with ALMA and CCAT.

Key words: galaxies: ISM – galaxies: nuclei – galaxies: starburst – infrared: galaxies

Online-only material: color figures, machine-readable table

1. INTRODUCTION

Systematic spectroscopic observations of far-infrared (FIR) cooling lines in large samples of local star-forming galaxies and active galactic nuclei (AGNs) were first carried out with the *Infrared Space Observatory* (*ISO*; e.g., Malhotra et al. 1997, 2001; Luhman et al. 1998; Brauher et al. 2008). These studies showed that [C II]157.7 μm is the most intense FIR emission line observed in normal, star-forming galaxies (Malhotra et al. 1997) and starbursts (e.g., Nikola et al. 1998; Colbert et al. 1999), dominating the gas cooling of their neutral interstellar medium (ISM). This fine-structure line arises from the $^2P_{3/2} \rightarrow {}^2P_{1/2}$ transition ($E_{ul}/k = 92$ K) of singly ionized Carbon atoms (ionization potential = 11.26 eV and critical density,

$n_{\rm H}^{\rm cr} \simeq 2.7\times10^3$ cm^{-3}; $n_{\rm e^-}^{\rm cr} \simeq 46$ cm^{-3}) which are predominantly excited by collisions with neutral hydrogen atoms; or with free electrons and protons in regions where $n_{\rm e^-}/n_{\rm H} \gtrsim 10^{-3}$ (Hayes & Nussbaumer 1984). Ultraviolet (UV) photons with energies >6 eV emitted by newly formed stars are able to release the most weakly bound electrons from small dust grains via photo-electric heating (Watson 1972; Draine 1978). In particular, polycyclic aromatic hydrocarbons (PAHs) are thought to be an important source of photo-electrons (Helou et al. 2001) that contribute, through kinetic energy transfer, to the heating of the neutral gas which subsequently cools down via collision with C^+ atoms and other elements in photo-dissociation regions (PDRs; Tielens & Hollenbach 1985; Wolfire et al. 1995).

The [C II]157.7 μm emission accounts, in the most extreme cases, for as much as ∼1% of the total IR luminosity of galaxies (Stacey et al. 1991; Helou et al. 2001). However, the [C II]/FIR ratio is observed to decrease by more than an order of magnitude in sources with high $L_{\rm IR}$ and warm dust temperatures ($T_{\rm dust}$). The underlying causes for these trends are still debated. The physical arguments most often proposed to explain the decrease in [C II]/FIR are: (1) self-absorption of the C^+ emission, (2) saturation of the [C II] line flux due to high density of the neutral gas, (3) progressive ionization of dust grains in high far-UV field to gas density environments, and (4) high dust-to-gas opacity caused by an increase of the average ionization parameter.

Although self-absorption has been used to explain the faint [C II] emission arising from warm, AGN-dominated systems such as Mrk 231 (Fischer et al. 2010), this interpretation has been questioned in normal star-forming galaxies due to the requirement of extraordinarily large column densities of gas in the PDRs (Luhman et al. 1998, Malhotra et al. 2001). Furthermore, contrary to the [O I] or [C I] lines, the [C II] emission is observed to arise from the external edges of those molecular clouds exposed to the UV radiation originated from starbursts, as for example in Arp 220 (Contini 2013). Therefore, self-absorption is not the likely explanation of the low [C II]/FIR ratios seen in most starburst galaxies, except perhaps in a few extreme cases, like NGC 4418 (Malhotra et al. 1997).

The [C II] emission becomes saturated when the hydrogen density in the neutral medium, $n_{\rm H}$, increases to values $\gtrsim 10^3$ cm^{-3}, provided that the far-UV (6–13.6 eV) radiation field is not extreme ($G_0 \lesssim 10^4$; where G_0 is normalized to the average local interstellar radiation field; Habing 1968). For example, for a constant $G_0 = 10^2$, an increase of the gas density from 10^4 to 10^6 cm^{-3} would produce a suppression of the [C II] emission of almost two orders of magnitude due to the rapid recombination of C^+ into neutral carbon and then into CO (Kaufman et al. 1999). However, PDR densities as high as 10^4 cm^{-3} are not very common. [O I]63.18 μm and [C II]157.7 μm *ISO* observations of normal star-forming galaxies and some IR-bright sources confine the physical parameters of their PDRs to a range of $G_0 \leqslant 10^{4.5}$ and $10^2 \lesssim n_{\rm H} \lesssim 10^4$ cm^{-3} (Malhotra et al. 2001). On the other hand, the [C II] emission can be also saturated when $G_0 > 10^{1.5}$ provided that $n_{\rm H} \lesssim 10^3$ cm^{-3}. In this regime, the line is not sensitive to an increase of G_0 because the temperature of the gas is well above the excitation potential of the [C II] transition.

It has also been suggested that in sources where $G_0/n_{\rm H}$ is high ($\gtrsim 10^2$ cm^3) the [C II] line is a less efficient coolant of the ISM because of the following reason. As physical conditions become more extreme (higher $G_0/n_{\rm H}$), dust particles progressively increase their positive charge (Tielens & Hollenbach 1985; Malhotra et al. 1997; Negishi et al. 2001). This reduces both the amount of photo-electrons released from dust grains that indirectly collisionally excite the gas, as well as the energy that they carry along after they are freed, since they are more strongly bounded. The net effect is the decreasing of the efficiency in the transformation of incident UV radiation into gas heating without an accompanied reduction of the dust emission (Wolfire et al. 1990; Kaufman et al. 1999; Stacey et al. 2010).

In a recent work, Graciá-Carpio et al. (2011) have shown that the deficits observed in several FIR emission lines ([C II]157.7 μm, [O I]63.18 μm, [O I]145 μm, and [N II]122 μm) could be explained by an increase of the average ionization parameter of the ISM, $\langle U \rangle$.[24] In "dust bounded" star-forming regions the gas opacity is reduced within the H II region due to the higher $\langle U \rangle$. As a consequence, a significant fraction of the UV radiation is eventually absorbed by large dust grains before being able to reach the neutral gas in the PDRs and ionize the PAH molecules (Voit 1992; González-Alfonso et al. 2004; Abel et al. 2009), causing a deficit of photo-electrons and hence the subsequent suppression of the [C II] line with respect to the total FIR dust emission.

Local luminous IR galaxies (LIRGs; $L_{\rm IR} = 10^{11-12}\,L_\odot$) are a mixture of single galaxies, disk galaxy pairs, interacting systems and advanced mergers, exhibiting enhanced star formation rates (SFRs), and a lower fraction of AGNs compared to higher luminous galaxies. A detailed study of the physical properties of low-redshift LIRGs is critical for our understanding of the cosmic evolution of galaxies and black holes since (1) IR-luminous galaxies comprise the bulk of the cosmic IR background and dominate star formation activity between $0.5 < z < 2$ (Caputi et al. 2007; Magnelli et al. 2011; Murphy et al. 2011; Berta et al. 2011) and (2) AGN activity may preferentially occur during episodes of enhanced nuclear star formation. Moreover, LIRGs are now assumed to be the local analogs of the IR-bright galaxy population at $z > 1$. However, a comprehensive analysis of the most important FIR cooling lines of the ISM in a complete sample of nearby LIRGs has not been possible until the advent of the *Herschel Space Observatory* (*Herschel* hereafter; Pilbratt et al. 2010) and, in particular, its Photodetector Array Camera and Spectrometer (PACS; Poglitsch et al. 2010).

In this work we present the first results obtained from *Herschel*/PACS spectroscopic observations of a complete sample of FIR selected local LIRGs that comprise the Great Observatories All-sky LIRG Survey (GOALS; Armus et al. 2009). Using this complete, flux-limited sample of local LIRGs, we are able for the first time to perform a systematic, statistically significant study of the FIR cooling lines of star-forming galaxies covering a wide range of physical conditions: from isolated disks where star formation is spread across kiloparsec scales to the most extreme environments present in late stage major mergers where most of the energy output of the system comes from its central kiloparsec region. In particular, in this paper we focus on the [C II]157.7 μm line and its relation with the dust emission in LIRGs. We make use of a broad set of mid-IR diagnostics based on *Spitzer*/IRS spectroscopy, such as high ionization emission lines, silicate dust opacities, PAH equivalent widths (EW), dust luminosity concentrations, and mid-IR colors, to provide the context in which the observed [C II] emission and [C II]/FIR

[24] The ionization parameter is defined as $U \equiv Q({\rm H})/4\pi R^2 n_{\rm H} c$, where Q(H) is the number of hydrogen ionizing photons, R is the distance of the ionizing source to the PDR, $n_{\rm H}$ is the atomic hydrogen density, and c is the speed of light. If an average stellar population and size for the star-forming region is assumed, then $U \propto G_0/n_{\rm H}$.

ratios are best explained. The paper is organized as follows: In Section 2 we present the LIRG sample and the observations. In Section 3 we describe the processing and analysis of the data. The results are presented in Section 4. In Section 5 we put in context our findings with recent results from intermediate- and high-redshift surveys started to be carried out by ALMA and in the future by Cornell–Caltech Atacama Telescope (CCAT). The summary of the results is given in Section 6.

2. SAMPLE AND OBSERVATIONS

2.1. The GOALS Sample

The GOALS (Armus et al. 2009) encompasses the complete sample of 202 LIRGs and ULIRGs contained in the *IRAS* Revised Bright Galaxy Sample (RBGS; Sanders et al. 2003) which, in turn, is also a complete sample of 629 galaxies with *IRAS* $S_{60\,\mu m} > 5.24$ Jy and Galactic latitudes $|b| > 5^{\circ}$. There are 180 LIRGs and 22 ULIRGs in GOALS and their median redshift is $z = 0.0215$ (or ∼95.2 Mpc), with the closest galaxy being at $z = 0.0030$ (15.9 Mpc; NGC 2146) and the farthest at $z = 0.0918$ (400 Mpc; IRAS 07251−0248). To date, there are many published and ongoing works that have already exploited the potential of all the multi-wavelength data available for this sample including, among others, *Galaxy Evolution Explorer* UV (Howell et al. 2010), *Hubble Space Telescope* optical and near-IR (Haan et al. 2011; Kim et al. 2013), and *Chandra* X-ray (Iwasawa et al. 2011) imaging, as well as *Spitzer*/IRS mid-IR spectroscopy (Díaz-Santos et al. 2010, 2011; Petric et al. 2011; Stierwalt et al. 2013; S. Stierwalt, in preparation; Inami et al. 2013), as well as a number of ground-based observatories (Very Large Array, CARMA, etc.) and soon ALMA.

The RBGS, and therefore the GOALS sample, were defined based on *IRAS* observations. However, the higher angular resolution achieved by *Spitzer* allowed us to spatially disentangle galaxies that belong to the same LIRG system into separate components. From the 291 *individual* galaxies in GOALS, not all have *Herschel* observations. In systems with two or more galactic nuclei, minor companions with MIPS 24 μm flux density ratios smaller than 1:5 with respect to the brightest galaxy were not requested since their contribution to the total IR luminosity of the system is small. Because the angular resolution of *Spitzer* decreases with wavelength, it was not possible to obtain individual MIPS 24, 70 and 160 μm measurements for all GOALS galaxies, and therefore to derive uniform IR luminosities for them using *Spitzer* data only. Instead, to calculate the individual, spatially integrated $L_{\rm IR}$ of LIRGs belonging to a system of two or more galaxies, we distributed the $L_{\rm IR}^{8-1000\,\mu m}$ of the system as measured by *IRAS* (using the prescription given in Sanders & Mirabel 1996) proportionally to the individual MIPS 70 μm flux density of each component when available, or to their MIPS 24 μm otherwise.[25] We will use these measurements of $L_{\rm IR}$ in Section 5.

2.2. Herschel/PACS Observations

We have obtained FIR spectroscopic observations for 153 LIRG systems of the GOALS sample using the Integral Field Spectrometer (IFS) of the PACS instrument on board *Herschel*. The data were collected as part of an OT1 program (OT1_larmus_1; P.I.: L. Armus) awarded with more than 165 hr of observing time. In this work will focus mainly on the analysis and interpretation of the [C II] observations of our galaxy sample. PACS range spectroscopy of the [C II]157.7 μm fine-structure emission line was obtained for 163 individual sources. Our observations were complemented with the inclusion of the remaining LIRGs in the GOALS sample for which [C II] observations are publicly available in the archive (as of 2012 October) from various *Herschel* projects. The main programs from which these data were gathered are: KPGT_esturm_1 (P.I.: E. Sturm), KPOT_pvanderw_1 (P.I.: P. van der Werf), and OT1_dweedman_1 (P.I.: D. Weedman). The total number of LIRG systems for which there are [C II] data is 200 (IRASF08339+6517 and IRASF09111−1007 were not observed). However, because some LIRGs are actually systems of galaxies (see above), the number of observed galaxies was 241.

The IFS on PACS is able to perform simultaneous spectroscopy in the 51–73 or 70–105 μm (third and second orders, respectively; "blue" camera) and the 102–210 μm (first order; "red" camera) ranges. The integral field unit (IFU) is composed by a 5 × 5 array of individual detectors (spaxels) each of one with a field of view (FoV) of ∼9.″4, for a total of 47″ × 47″. The physical size of the PACS FoV at the median distance of our LIRG sample is ∼20 kpc on a side. The number of spectral elements in each pixel is 16, which are rearranged together via an image slicer over two 16 × 25 Ge:Ga detector arrays (blue and red cameras).

Our Astronomical Observation Requests were consistently constructed using the "Range" spectroscopy template, which allows the user to define a specific wavelength range for the desired observations. Our selected range was slightly larger than that provided by default for the "Line" mode. This was necessary (1) to obtain parallel observations of the wide OH 79.18 μm absorption feature using the blue camera when observing the [C II]157.7 μm line, and (2) to ensure that the targeted emission lines have a uniform signal-to-noise ratio (S/N) across their spectral profiles even if they are to be broader than a few hundred km s^{-1}. The high sampling density mode scan, useful to have sub-spectral resolution information of the lines (see below), was employed. While we requested line maps for some LIRGs of the sample (from two to a few raster positions depending on the target), pointed (one single raster) chop-nod observations were taken for the majority of galaxies. For those galaxies with maps, only one raster position was used to obtain the line fluxes used in this work. The chopper throw varied from small to large depending on the source. Spectroscopy of the LIRGs included in GOALS but observed by other programs in [C II] was not always obtained using the "Range" mode but some of them were observed using "LineScan" spectroscopy. The S/N of the data varies not only from galaxy to galaxy but also depending on the emission line considered. We provide uncertainties for all quantities used across the analysis presented here that are based on the individual spectrum of each line, therefore reflecting the errors associated with—and measured directly on—the data.

2.3. Spitzer/IRS Spectroscopy

As part of the *Spitzer* GOALS legacy, all galaxies observed with *Herschel*/PACS have available *Spitzer*/IRS low resolution ($R \sim 60$–120) slit spectroscopy (SL module: 5.5–14.5 μm, and LL module: 14–38 μm). The 244 IRS spectra were extracted using the standard extraction aperture and point source calibration mode in SPICE. The projected angular sizes of the apertures on the sky are 3.″7 × 12″ at the average wavelength of 10 μm in

[25] There are two systems for which no individual MIPS 24 μm fluxes could be obtained. In these cases their IRAC 8 μm emission was used for scaling the $L_{\rm IR}$. These LIRGs are MCG+02-20-003 and VV250a.

SL and 10.″6 × 35″ at the average wavelength of 26 μm in LL. Thus, the area covered by the SL aperture is approximately equivalent (within a factor of ∼2) to that of an individual spaxel of the IFS in PACS, and so is that of the LL aperture to a 3 × 3 spaxel box. The observables derived from the Infrared Spectrograph (IRS) data that we use in this work are the strength of the 9.7 μm silicate feature, $S_{9.7\,\mu\mathrm{m}}$, and the EW of the 6.2 μm PAH, which were presented in Stierwalt et al. (2013). We refer the reader to this work for further details about the reduction, extraction, calibration, and analysis of the spectra.

3. IFS/PACS DATA REDUCTION AND ANALYSIS

3.1. Data Processing

The *Herschel* Interactive Processing Environment (HIPE; ver. 8.0) application was used to retrieve the raw data from the *Herschel* Science Archive[26] as well as to process them. We used the script for "LineScan" observations (also valid for "Range" mode) included within HIPE to reduce our spectra. We processed the data from level 0 up to level 2 using the following steps: flag and reject saturated data, perform initial calibrations, flag and reject "glitches," compute the differential signal of each on–off pair of data-points for each chopper cycle, calculate the relative spectral response function, divide by the response, convert frames to PACS cubes, and correct for flat-fielding (this extra step is included in ver. 8.0 of HIPE and later versions, and helps to improve the accuracy of the continuum level). Next, for each camera (red or blue), HIPE builds the wavelength grid, for which we chose a final rebinning with an *oversample* = 2, and an *upsample* = 3 that corresponds to a Nyquist sampling. The spectral resolution achieved at the position of the [C II]157.7 μm line was derived directly from the data and is ∼235 km s^{-1}. The final steps are: flag and reject remaining outliers, rebin all selected cubes on consistent wavelength grids and, finally, average the nod-A and nod-B rebinned cubes (all cubes at the same raster position are averaged). This is the final science-grade product currently possible for single raster observations. From this point on, the analysis of the spectra was performed using in-house developed IDL routines.

3.2. Data Analysis

To obtain the [C II] flux of a particular source we use an iterative procedure to find the line and measure its basic parameters. First, we fit a linear function to the continuum emission, which is evaluated at the edges of the spectrum, masking the central 60% of spectral elements (where the line is expected to be detected) and without using the first and final 10%, where the noise is large due to the poor sampling of the scanning. Then, we fit a Gaussian function to the continuum-subtracted spectrum and calculate its parameters. We define a line as not detected when the peak of the Gaussian is below 2.5 times the standard deviation of the continuum, as measured in the previous step. On the other hand, if the line is found, we return to the original, total spectrum and fit again the continuum using this time a wavelength range determined by the two portions of the spectrum adjacent to the line located beyond $\pm 3\sigma$ from its center (where σ is the width of the fitted Gaussian) and the following ±15% of spectral elements. We then subtract this continuum from the total spectrum and fit the line again. The new parameters of the Gaussian are compared with the previous ones. This process is repeated until the location, sigma, and intensity of the line converge with an accuracy of 1%, or when reaching 10 iterations. Due to the merger-driven nature of many LIRGs, their gas kinematics are extremely complicated and, as a consequence, the emission lines of several sources present asymmetries and double peaks in their profiles. However, despite the fact that the width determined by the fit is not an accurate representation of the real shape of the line, it can be used as a first order approximation for its broadness. Therefore, instead of using the parameters of the Gaussian to derive the flux of the line, we decided to integrate directly over the final continuum-subtracted spectrum within the $\pm 3\sigma$ region around the central position of the line. The associated uncertainty is calculated as the standard deviation of the latest fitted continuum, integrated over the same wavelength range as the line. Absolute photometric uncertainties due to changes in the PACS calibration products are not taken into account (the version used in this work was PACS_CAL_32_0).[27]

We obtained the line fluxes for our LIRGs from the spectra extracted from the spaxel at which the [C II] line + continuum emission of each galaxy peaks within the PACS FoV. The *Spitzer*/IRS and *Herschel* pointings usually coincide within $\lesssim$2″. There are a few targets for which the IRS pointing is located more than half a spaxel away from that of PACS. In these cases, we decided to obtain the nuclear line flux of the galaxy by averaging the spaxels closest to the coordinates of the IRS pointing. These values are used only when PACS and IRS measurements are compared directly in the same plot. There is one additional LIRG system, IRAS 03582+6012, for which the PACS pointing exactly felt in the middle of two galaxies separated by only 5″. This LIRG is not used in the comparisons of the [C II] emission to the IRS data since the two individual sources cannot be disentangled.

As mentioned in Section 2.3, the angular size of a PACS spaxel is roughly similar (within a factor of two) to that of the aperture used to extract the *Spizer*/IRS spectra of our galaxies. Because the PACS beam is under-sampled at 160 μm (FWHM ∼ 12″ compared with the 9.″6 size of the PACS spaxels), and most of the sources in the sample are unresolved at 24 μm in our MIPS images (which have a similar angular resolution as PACS at ∼80 μm), an aperture correction has to be performed to the spectra extracted from the emission-peak spaxel of each galaxy to obtain their total nuclear fluxes. This was the same procedure employed to obtain the mid-IR IRS spectra of our LIRGs. The nominal, wavelength-dependent aperture correction function provided by HIPE ver. 8.0 works optimally when the source is exactly positioned at the center of a given spaxel. However, in some occasions the pointing of *Herschel* is not accurate enough to achieve this and the target can be slightly misplaced $\lesssim$3″ (up to 1/3 of a spaxel) from the center. In these cases, the flux of the line might be underestimated. We explored whether this effect could be corrected by measuring the position of the source within the spaxel. However, some LIRGs in our sample show low surface-brightness extended emission, either because of their proximity and/or merger nature, or simply because the gas and dust emission are spatially decoupled. This, combined with the spatial sub-sampling of the PACS/IFS detector and the poor S/N of some sources prevented us from obtaining an accurate measurement of the spatial position and angular width of the [C II] emission and therefore from obtaining a more refined aperture correction. Thus, we performed only the nominal aperture correction provided by HIPE.

[26] http://herschel.esac.esa.int/Science_Archive.shtml

[27] http://herschel.esac.esa.int/twiki/bin/view/Public/PacsCalTreeHistory

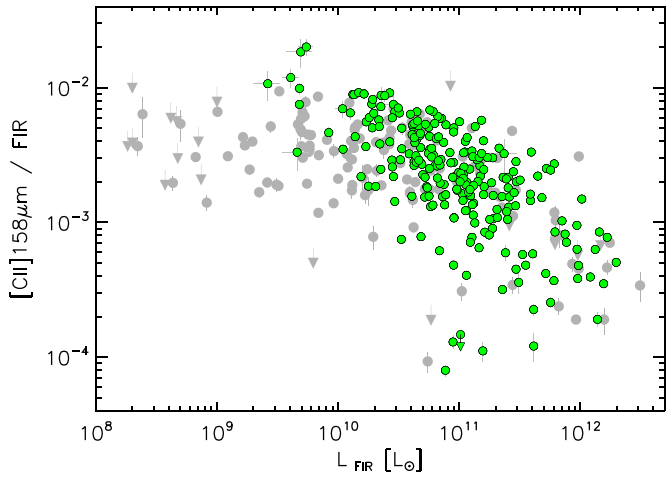

Figure 1. Ratio of [C II]157.7 μm to FIR flux as a function of the FIR luminosity for individual galaxies in the GOALS sample (green circles) and for unresolved galaxies observed with *ISO* (gray circles and limits) obtained from the compilation of Brauher et al. (2008) located at $z > 0.003$, similar to the distance range covered by our LIRGs. The $L_{\rm FIR}$ of galaxies was calculated as explained at the end of Section 3.2 and covers the 42.5–122.5 μm wavelength range as defined in Helou et al. (1988).

(A color version of this figure is available in the online journal.)

The *IRAS* FIR fluxes used throughout this paper were calculated as FIR $= 1.26 \times 10^{-14}\,(2.58\,S_{60\,\mu\rm m} + S_{100\,\mu\rm m})$ (W m^{-2}), with S_ν in (Jy). The FIR luminosities, $L_{\rm FIR}$, were defined as $4\pi\ D_{\rm L}^2$ FIR ($L_\odot$). The luminosity distances, $D_{\rm L}$, were taken from Armus et al. (2009). This definition of the FIR accounts for the flux emitted within the 42.5–122.5 μm wavelength range as originally defined in Helou et al. (1988). The FIR fluxes and luminosities of galaxies were then matched to the aperture with which the nuclear [C II] flux was extracted (see above) by scaling the integrated *IRAS* FIR flux of the LIRG system with the ratio of the continuum flux density of each individual galaxy evaluated at 63 μm in the PACS spectrum (extracted at the same position and with the same aperture as the [C II] line) to the total *IRAS* 60 μm flux density of the system.

In Table 1 we present the [C II]157.7 μm flux, the [C II]/FIR ratio, and the continuum flux densities at 63 and 158 μm for all the galaxies in our sample. Future updates of the data in this table processed with newer versions of HIPE and PACS calibration files will be available at the GOALS Web site: http://goals.ipac.caltech.edu.

4. RESULTS AND DISCUSSION

4.1. The [C II]/FIR Ratio: Dust Heating and Cooling

The FIR fine-structure line emission in normal star-forming galaxies as well as in the extreme environments hosted by ULIRGs has been extensively studied for the past two decades. A number of works based on *ISO* data already suggested that the relative contribution of the [C II]157.7 μm line to the cooling of the ISM in PDRs compared to that of large dust grains, as gauged by the FIR emission, diminishes as galaxies are more IR luminous (Malhotra et al. 1997; Luhman et al. 1998; Brauher et al. 2008). Figure 1 display the classical plot of the [C II]/FIR ratio as a function of the FIR luminosity for our LIRG sample. In addition, we also show for reference those galaxies observed with *ISO* compiled by Brauher et al. (2008) that are classified as unresolved and located at redshifts $z > 0.003$, similar to the distance range covered by GOALS. As we can see, our *Herschel* data confirm the trend seen with *ISO* by which galaxies with $L_{\rm FIR} \gtrsim 10^{11}\ L_\odot$ show a significant decrease of the [C II]/FIR ratio. GOALS densely populates this critical part of phase-space providing a large sample of galaxies with which to explore the physical conditions behind the drop in [C II] emission among LIRGs. For the 32 galaxies with measurements obtained with both telescopes, the higher angular resolution *Herschel* observations of the nuclei of LIRGs are able to recover an average of ~87% of the total [C II] flux measured by *ISO*.

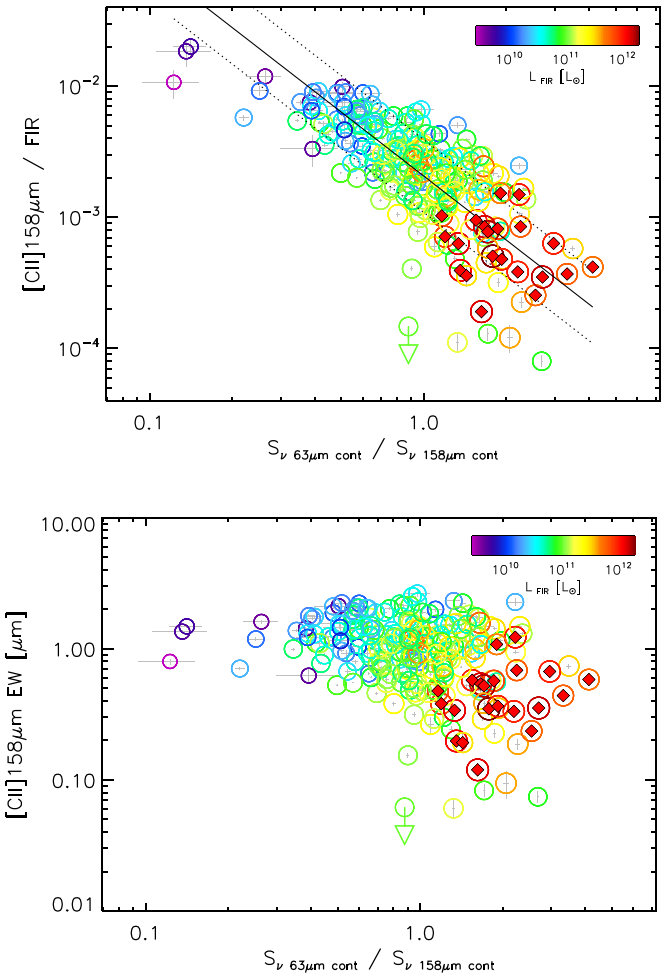

Figure 2. Ratio of [C II]157.7 μm to FIR flux (upper panel) and [C II]157.7 μm EW (bottom panel) as a function of the S_ν 63 μm/S_ν 158 μm continuum flux density ratio for individual galaxies in the GOALS sample. Circles of different colors indicate the $L_{\rm FIR}$ of galaxies (see color bar), which is defined as explained in Section 3.2. Red diamonds mark galaxies with $L_{\rm IR} \geqslant 10^{12}\ L_\odot$, ULIRGs. These two plots show that the decrease of the [C II]/FIR ratio with warmer FIR colors seen in our LIRGs is primarily caused by a significant decrease of gas heating efficiency and an increase of warm dust emission. The solid line in the upper panel corresponds to a linear fit of the data in log–log space. The parameters of the fit are given in Equation (1). The dotted lines are the $\pm 1\sigma$ uncertainty.

(A color version of this figure is available in the online journal.)

4.1.1. The Average Dust Temperature of LIRGs

Figure 2 (upper panel) shows the [C II]157.7 μm/FIR ratio for the GOALS sample as a function of the FIR PACS S_ν 63 μm/S_ν 158 μm continuum flux density ratio. We chose to use this PACS-based FIR color in the *x*-axis instead of the more common *IRAS* 60/100 μm color mainly because of two main reasons: (1) this way we are able plot data from individual galaxies instead of being constrained by the spatial resolution of *IRAS*,

Table 1
Herschel/PACS Measurements for the GOALS Sample

Galaxy Name (1)	R.A. (hh:mm:ss) (2)	Decl. (dd:mm:ss) (3)	Dist. (Mpc) (4)	[C II]157.7 μm ($\times10^{-15}$ W m^{-2}) (5)	[C II]/FIR ($\times10^{-3}$) (6)	S_ν63 μm cont. (Jy) (7)	S_ν158 μm cont. (Jy) (8)
NGC 0023	$00^h09^m53\overset{s}{.}4$	$+25°55^m26^s$	65.2	1.385 ± 0.022	4.13 ± 0.09	6.17 ± 0.08	6.85 ± 0.08
NGC 0034	$00^h11^m06\overset{s}{.}5$	$-12°06^m26^s$	84.1	0.624 ± 0.018	0.85 ± 0.03	16.39 ± 0.13	9.02 ± 0.06
Arp256	$00^h18^m50\overset{s}{.}9$	$-10°22^m36^s$	117.5	0.967 ± 0.020	2.96 ± 0.07	6.70 ± 0.08	4.42 ± 0.09
...	...	...	...	...	...	...	...

Notes. Columns: (1) galaxy name; (2) and (3) right ascension and declination (J2000) of the position from which the *Herschel*/PACS spectrum was extracted (Section 3.2); (4) distance to the galaxies taken from Armus et al. (2009); (5) [C II]157.7 μm flux as measured from the spaxel at which the [C II] line + continuum emission of the galaxy peaks within the PACS FoV, that is, within an effective aperture of $\sim9\overset{''}{.}4 \times 9\overset{''}{.}4$ (Section 3.2); (6) [C II] to FIR flux ratio, where the FIR fluxes have been scaled to match the aperture of the [C II] measurements; (7) continuum flux density at 63 μm under the [O I] line extracted at the same position and with the same aperture size as (5); (8) same as (7) but for the continuum at 158 μm under the [C II] line. There are 11 galaxies for which the *Spitzer*/IRS pointing is located $>4\overset{''}{.}7$ from the position of the [C II]+continuum peak. For these, we include an extra entry in the table with the [C II] flux and continuum measurements obtained at the position of the IRS slit. They are marked with asterisks next to the names.
Future, updated versions of these data can be found at the GOALS Web site: http://goals.ipac.caltech.edu.

(This table is available in its entirety in a machine-readable form in the online journal. A portion is shown here for guidance regarding its form and content.)

which would force us to show only blended sources; (2) by using the 63/158 μm ratio we are probing a larger range of dust temperatures within the starburst ($T \sim 50 \rightarrow 20$ K); with the colder component probably arising from regions located far from the ionized gas-phase, and closer to the PDRs where the [C II] emission originates. For reference, we show the relation between the PACS 63/158 μm and *IRAS* 60/100 μm colors in the Appendix. The ULIRGs in the GOALS sample (red diamonds) have a median [C II]/FIR $= 6.3 \times 10^{-4}$, a mean of $6.6\,(\pm0.8) \times 10^{-4}$, and a standard deviation of the distribution of 3.7×10^{-4}. LIRGs span two orders of magnitude in [C II]/FIR, from $\sim10^{-2}$ to $\sim10^{-4}$, with a mean of 3.4×10^{-3} and a median of 2.6×10^{-3}. The $L_{[\rm C\,II]}$ ranges from $\sim10^7$ to 2×10^9 $L_\odot$.

Our results are consistent with *ISO* observations of a sample of normal and moderate IR-luminous galaxies presented in Malhotra et al. (1997) and further analyzed in Helou et al. (2001). The GOALS sample, though, populates a warmer FIR color regime. Despite the increase in dispersion at 63/158 μm $\gtrsim$ 1.25 or [C II]157.7 μm/FIR $\lesssim 10^{-3}$ (basically in the ULIRG domain), the fact that we find the same tight trend independently of the range of IR luminosities covered by the two samples suggests that the main observable linked to the variation of the [C II]/FIR ratio is the average temperature of the dust ($T_{\rm dust}$) in galaxies.

This interpretation agrees with the last physical scenario described in the Introduction, in which an increase of the ionization parameter, $\langle U \rangle$, would cause the far-UV radiation from the youngest stars to be less efficient in heating the gas in those galaxies. At the same time, dust grains would be on average at higher temperatures due to the larger number of ionizing photons per dust particle available in the outer layers of the H II regions, close to the PDRs. Indeed, the presence of dust within H II regions has been recently observed in several star-forming regions in our Galaxy (Paladini et al. 2012). Both effects combined can explain the wide range of [C II]157.7 μm/FIR ratios and FIR colors we observe in the most warm LIRGs. Variations in $n_{\rm H}$, though, could be responsible for the dispersion in [C II]/FIR seen at a given 63/158 μm ratio.

To further support these findings, the bottom panel of Figure 2 shows that the ratio of [C II]157.7 μm flux to the monochromatic continuum at $\sim$158 μm under the line (the [C II] EW) of the warmest galaxies is only a factor of $\sim$4 lower than the average [C II] EW displayed by colder sources at 63/158 μm $\lesssim 1$. This implies that the decrease of the [C II]/FIR ratio seen in our LIRGs is primarily caused by a significant increase in warm dust emission (peaking at $\lambda \lesssim$ 60–100 μm), most likely associated with the youngest stars, that is not followed by a proportional enhancement of the [C II] emission line.

The best fit to the data in Figure 2 (upper panel) yields the following parameters:

$$\log\left(\frac{[\rm C\,II]}{\rm FIR}\right) = -2.68(\pm0.02) - 1.61(\pm0.09)\log\left(\frac{S_{63\,\mu\rm m}}{S_{158\,\mu\rm m}}\right) \quad (1)$$

with a dispersion of 0.28 dex. We note that the [C II]/FIR ratios predicted by the fitted relation for sources with FIR colors 63/158 μm $\lesssim$ 0.4 are probably overestimated, as it is already know that galaxies showing such cool $T_{\rm dust}$ have typical [C II]/FIR $\sim 10^{-2}$ (e.g., Malhotra et al. 2001).

4.1.2. The Link between Mid-IR Dust Obscuration and FIR Re-emission

The strength of the 9.7 μm silicate feature is defined as $S_{9.7\,\mu\rm m} \equiv \ln(f^{\rm obs}_{\lambda_P}/f^{\rm cont}_{\lambda_P})$; with $f^{\rm cont}_{\lambda_P}$ and $f^{\rm obs}_{\lambda_P}$ being the unobscured and observed continuum flux density measured in the mid-IR IRS spectra of our LIRGs and evaluated at the peak of the feature, λ_P, normally at 9.7 μm (see Stierwalt et al. 2013 for details on how it was calculated in our sample). Negative values indicate absorption, while positive ones indicate emission. By definition, $S_{9.7\,\mu\rm m}$ measures the apparent optical depth toward the warm, mid-IR emitting dust. Figure 3 shows that there is a clear trend ($r = 0.65$, $p_r = 0$; $\kappa = 0.47$) for LIRGs with stronger (more negative) $S_{9.7\,\mu\rm m}$ to display smaller [C II]/FIR ratios, implying that the dust responsible for the mid-IR absorption is also accountable for the FIR emission. The formal fit (solid line) can be expressed as:

$$\log\left(\frac{[\rm C\,II]}{\rm FIR}\right) = -2.32(\pm0.02) + 0.83(\pm0.05)\,S_{9.7\,\mu\rm m} \quad (2)$$

with a dispersion in the y-axis of 0.30 dex.

Within the context described in the previous section, the contrast between the inner layer of dust that is being heated by the ionizing radiation to $T \gtrsim 50$ K and that of the cold dust at $T \lesssim 20$ K emitting at $\lambda \gtrsim 150\,\mu$m would create

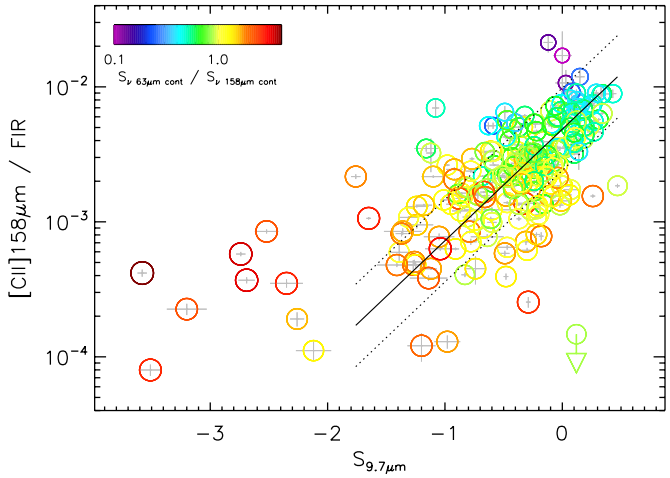

Figure 3. [C II]157.7 μm/FIR ratio for individual galaxies in the GOALS sample as a function of the strength of the 9.7 μm silicate absorption feature, $S_{9.7\,\mu m}$, measured with *Spitzer*/IRS. Galaxies are color-coded as a function of the S_ν 63 μm/S_ν 158 μm ratio, with values ranging from 0.10 to 4.15 (see Figure 2). The solid line represents an outlier-resistant fit to the bulk of the star-forming LIRG population with $S_{9.7\,\mu m} \geqslant -2$. The dotted lines are the $\pm 1\sigma$ uncertainty. (A color version of this figure is available in the online journal.)

both (1) the silicate absorption seen at 9.7 μm due to the larger temperature gradient between the two dust components and (2) the increasingly higher 63/158 μm ratios seen in Figure 2 due to the progressively larger amount of dust mass that is being heated to higher temperatures. This scenario is consistent with the physical properties of the ISM found in the extreme environments of ULIRGs, in which the fraction of total dust luminosity contributed by the diffuse ISM decreases significantly, and the emission from dust at $T \sim 50$–60 K arising from optically thick "birth clouds" (with ages $\lesssim 10^{7-8}$ Myr) accounts for $\gtrsim$80% of their IR energy output (da Cunha et al. 2010). Furthermore, our findings are also in agreement with recent results showing that the increase of the silicate optical depth in LIRGs is related with the flattening of their radio spectral index (1.4 to 8.44 GHz) due to an increase of free–free absorption, suggesting that the dust obscuration must largely be originated in the vicinity and/or within the starburst region (Murphy et al. 2013).

There are a few galaxies that do not follow the correlation fitted in Figure 3, showing very large silicate strengths ($S_{9.7\,\mu m} < -2$) and small [C II]/FIR ratios ($<10^{-3}$) typical of ULIRGs or, in general, warm galaxies (see color coding or Figure 2). We would like to note that the trend found for the majority of our sample only reaches $S_{9.7\,\mu m}$ values up to around -1.5 which, interestingly, is only slightly larger than the apparent optical depth limit that a obscuring clumpy medium can explain (Nenkova et al. 2008). Larger (more negative) values of the silicate strength can only be achieved by a geometrically thick (smooth) distribution of cold dust, suggesting that the extra dust absorption seen in these few galaxies may not be related with the star-forming region from where the [C II] and FIR emissions arise.

But then, what is the origin of this excess of obscuration? One possibility is that it is caused by foreground cold dust not associated with the starburst. This has been seen in some heavily obscured Compton-thick AGNs, where most of the deep silicate absorption measured in these objects seems to originate from dust located in the host galaxy (Goulding et al. 2012; González-Martín et al. 2012). Alternatively, the presence of an extremely warm source (different from the star-forming region(s) that are producing the FIR and [C II] emission) could contribute with additional emission of hot dust ($T \gtrsim 150$ K) to the mid-IR. If at the same time this source is deeply buried (optically thick) and embedded in layers of progressively colder dust (geometrically thick), it could produce a cumulative absorption that we would measure via the strength of the silicate feature while still contributing to the emission outside of it (see Levenson et al. 2007; Sirocky et al. 2008).

While both explanations are plausible, the second is favored by the fact that these extremely obscured galaxies show MIPS 24/70 μm ratios very similar, or even slightly higher than those found for the rest of the LIRGs in the sample. If foreground cold dust was the responsible for the excess of obscuration, we would expect these galaxies to show abnormally low 24 μm luminosities with respect to the FIR. We find that this is not the case, in agreement with recent results based on radio observations of a sub-sample of LIRGs in GOALS (Murphy et al. 2013). Furthermore, the existence of an additional hot and obscured dust component in these LIRGs is also consistent with the results presented in Stierwalt et al. (2013), where it is shown that there is a trend for LIRGs with moderate silicate strengths ($S_{9.7\,\mu m} \gtrsim -1.5$) to show higher S_ν 30 μm/S_ν 15 μm ratios as the $S_{9.7\,\mu m}$ becomes stronger (more negative). That is, more obscured LIRGs have increasingly larger fluxes at 30 μm, in agreement with our findings in the previous section. However, galaxies showing the most extreme silicate strengths ($S_{9.7\,\mu m} < -1.5$) do not have proportionally higher 30/15 μm ratios. On the contrary, they show ratios similar to those of warm LIRGs with mild silicate strengths (or even lower than expected given their extreme $S_{9.7\,\mu m}$), supporting the idea that in these particular galaxies the dust producing this additional absorption and excess of mid-IR emission ($\lambda \lesssim 20\,\mu$m) represents a component of the overall nuclear starburst activity different than the star-forming regions that drive the FIR cooling.

4.1.3. The Compactness of the Mid-IR Emitting Region

The compactness of the starburst region of a galaxy has been proven to be related to many of its other physical properties (Wang & Helou 1992). For example, all ULIRGs in the GOALS sample have very small mid-IR emitting regions, with sizes (measured FWHMs) <1.5 kpc (Díaz-Santos et al. 2010). LIRGs, on the other hand, span a large range in sizes as well as in how much of their mid-IR emission is extended. The later property is parameterized in Díaz-Santos et al. (2010) by the fraction of extended emission, FEE_λ, which measures the fraction of light emitted by a galaxy that is contained outside of its unresolved component at a given wavelength λ. The complementary quantity $1-\mathrm{FEE}_\lambda$ measures how compact the source is, which in turn is proportional to its luminosity surface density, Σ. We note that in this paper we use the word compactness as an equivalent to light concentration, i.e., as a measurement of the amount of energy per unit area produced by a source, and not as an absolute measurement of its size.

It has been shown that the compactness of the mid-IR continuum emission of LIRGs (evaluated at $\lambda_{\rm rest} = 13.2\,\mu$m) is related to their merger stage, mid-IR AGN-fraction and most importantly, to their FIR color (Díaz-Santos et al. 2010). LIRGs with higher *IRAS* S_ν 60 μm/S_ν 100 μm ratios are increasingly compact. In other words, for a given $L_{\rm IR}$, the dust in sources with FIR colors peaking at shorter wavelengths is not only hotter but also confined toward a smaller volume in the center of galaxies. In Section 4.1.1 we found that the [C II]/FIR ratio is related

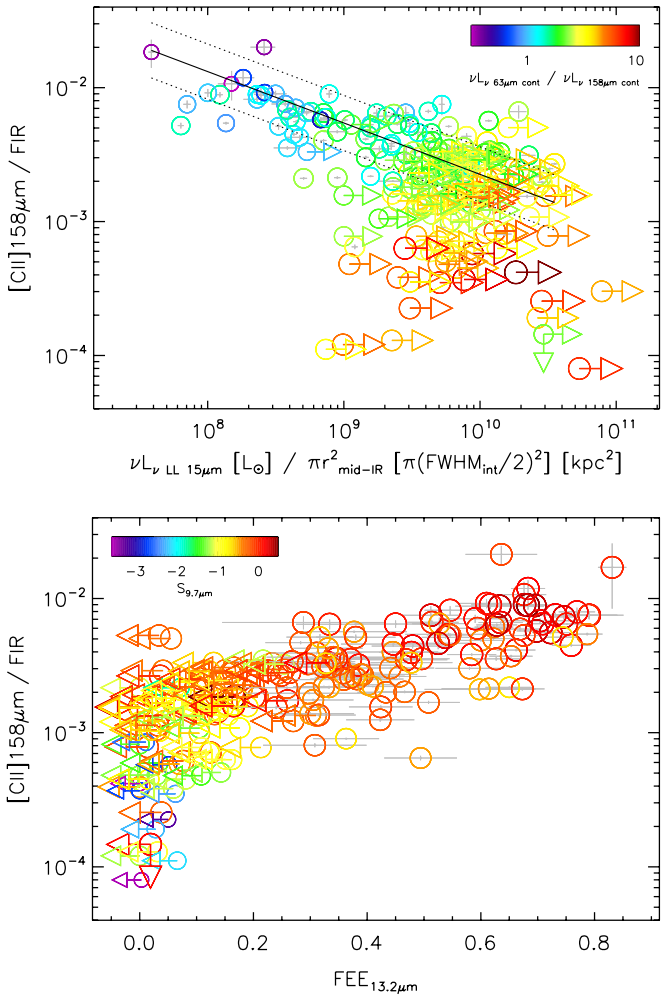

Figure 4. [C II]157.7 μm/FIR ratio as a function of the luminosity surface density at 15 μm, $\Sigma_{15\,\mu m}$ (top), and the fraction of extended emission at 13.2 μm, $FEE_{13.2\,\mu m}$ (bottom), for individual galaxies in the GOALS sample. Galaxies are color-coded as a function of the 63/158 μm ratio (top) and the strength of the silicate feature, $S_{9.7\,\mu m}$ (bottom). A linear fit to the datapoints without limits is shown in the top panel as a solid line. The dotted lines are the $\pm1\sigma$ uncertainty. We note that the 15 μm luminosities are measured within the *Spitzer*/IRS LL slit while the mid-IR sizes were obtained from the SL module at 13.2 μm (Díaz-Santos et al. 2010). For very extended sources, the MIPS 24 μm images were used instead to measure the size of the starburst region. The intrinsic sizes ($FWHM_{int}$) of the mid-IR emission were obtained after subtracting, in quadrature, the contribution of the instrumental profile ($FWHM_{PSF}$) from the measured FWHM.

(A color version of this figure is available in the online journal.)

to the average T_{dust} of our galaxies. Thus, we should expect to see a correlation between the [C II] deficit and the luminosity surface density and compactness of LIRGs in the mid-IR. This is shown in Figure 4, where a clear trend is found for galaxies with higher luminosity surface densities at 15 μm, $\Sigma_{15\,\mu m}$ (top panel), or small $FEE_{13.2\,\mu m}$ (bottom panel), i.e., more compact, to show lower [C II]/FIR ratios, irrespective of the origin of the nuclear power source.

Excluding those LIRGs for which only upper limits on their mid-IR size or $L_{[C\,II]}$ are available, we perform a linear fit to the data and obtain the following parameters for the correlation between [C II]/FIR and $\Sigma_{15\,\mu m}$:

$$\log\left(\frac{[C\,II]}{FIR}\right) = 1.19(\pm0.30) - 0.38(\pm0.03) \times \log(\Sigma_{15\,\mu m}) \quad (3)$$

with a dispersion in the y-axis of 0.21 dex.

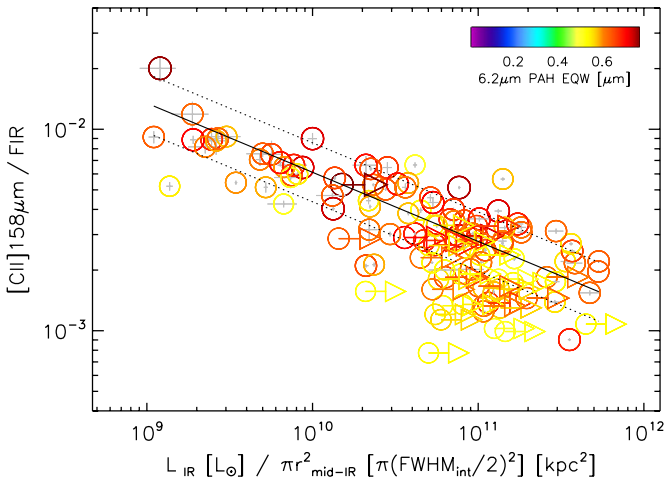

Figure 5. [C II]157.7 μm/FIR ratio as a function of the nuclear L_{IR} divided by the area of the mid-IR emitting region ($\Sigma_{IR} = L_{IR}/\pi r^2_{mid\text{-}IR}$) for individual galaxies in the GOALS sample. This figure is the same as Figure 4 but using the nuclear L_{IR} of galaxies (scaled as the FIR flux; see Section 3.2) instead of their 15 μm monochromatic luminosity, and it is color-coded as a function of the 6.2 μm PAH EW. Only pure star-forming LIRGs, defined as to have 6.2 μm PAH $\geqslant$ 0.5 μm, are shown. The solid line is a fit to the data. See Equation (4).

(A color version of this figure is available in the online journal.)

4.2. The Role of Active Galactic Nuclei

It is known that the contribution of an AGN to the IR emission in LIRGs increases with L_{IR} (Veilleux et al. 1995; Desai et al. 2007; Petric et al. 2011; Alonso-Herrero et al. 2012). This is most noticeable at mid-IR wavelengths (Laurent et al. 2000; Armus et al. 2007; Mullaney et al. 2011) but a non-negligible fraction of the FIR emission of ULIRGs can also be powered by an AGN. The EW of mid-IR PAH features is a simple diagnostic that has been widely used for the detection of AGN activity in galaxies at low and high redshifts (Genzel et al. 1998; Armus et al. 2007; Desai et al. 2007; Spoon et al. 2007; Pope et al. 2008; Murphy et al. 2009; Menéndez-Delmestre et al. 2009; Veilleux et al. 2009; Petric et al. 2011; Stierwalt et al. 2013). Broadly speaking, the PAH EW decreases as a component of hot dust at $T \gtrsim 300$ K, normally ascribed to an AGN, starts to increasingly dominate the mid-IR continuum emission of the galaxy. In addition, the hard radiation field of an AGN could be able to destroy a significant fraction of the smallest PAH molecules (Voit 1992; Siebenmorgen et al. 2004). In particular, a galaxy is regarded as mid-IR AGN-dominated when its 6.2 μm PAH EW $\lesssim 0.3$, and it is classified as a pure starburst when 6.2 μm PAH EW $\gtrsim 0.5$ (although these limits are not strict). Sources with intermediate values are considered composite galaxies, in which both starburst and AGN may contribute significantly to the mid-IR emission.

4.2.1. [C II]157.7 μm Deficit in Pure Star-Forming LIRGs

Figure 5 shows the [C II]/FIR ratio as a function of the IR luminosity surface density, Σ_{IR}, of the LIRGs in GOALS, color-coded as a function of their 6.2 μm PAH EW. As we can see, when only pure star-forming galaxies are considered (6.2 μm PAH EWs $\geqslant$ 0.5 μm), the [C II]/FIR ratio drops by an order of magnitude, from 10^{-2} to $\sim10^{-3}$. This indicates that the decrease in [C II]/FIR among the majority of LIRGs is not caused by a rise of AGN activity but instead is a fundamental property of the starburst itself. It is only in the most extreme cases, when [C II]/FIR $< 10^{-3}$, that the AGN could play a significant role. In fact, powerful AGNs do not always reduce

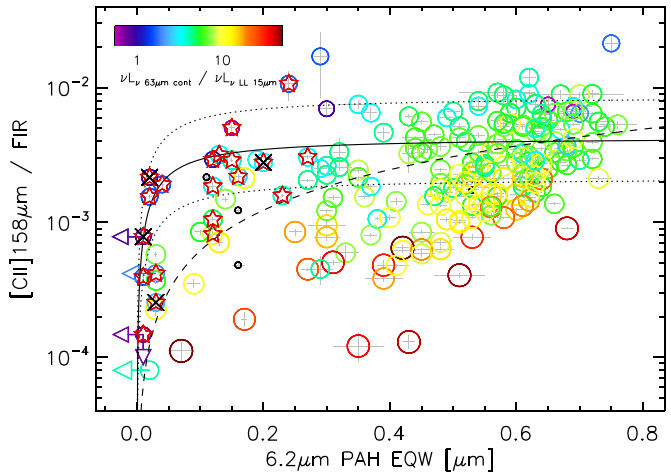

Figure 6. [C II]157.7 μm/FIR ratio for individual galaxies in the GOALS sample as a function of the 6.2 μm PAH EW measured with *Spitzer*/IRS. Galaxies are color-coded as a function of their νL_{ν} 63/15 μm ratio. If this information is not available, galaxies are shown as small black circles. The solid line represents the range in [C II]/FIR and 6.2 μm PAH with increasing contribution from an AGN (see text for details). The dotted lines are $\times 2$ and $\times 0.5$ the predicted trend, which accounts for variations in the [C II]/6.2 μm PAH ratio and the $L_{\rm FIR}/\nu L_{\nu\,6\,\mu{\rm m}}$ relation for star-forming galaxies. The dashed line assumes a decreasing of the [C II]/6.2 μm PAH ratio proportional to the 6.2 μm PAH EW due to pure PAH destruction from an AGN.

(A color version of this figure is available in the online journal.)

the [C II]/FIR ratio, as shown also in Sargsyan et al. (2012). Stacey et al. (2010) also find that the AGN-powered sources in their high-redshift galaxy sample display small [C II]/FIR ratios. However, they speculate that except for two blazars, the deficit seen in these sources could be caused compact, nuclear starbursts (with sizes less than 1–3 kpc) perhaps triggered by the AGN. We will return to this discussion in Section 4.2.2.

The result obtained above also implies that the [C II]157.7 μm line alone is not a good tracer of the SFR in most local LIRGs since it does not account for the increase of warm dust emission (Figure 2) seen in the most compact galaxies that is usually associated with the most recent starburst. In Figure 5 we fit the data to provide a relation between the [C II]/FIR ratio and the $\Sigma_{\rm IR}$ for pure star-forming LIRGs. The analytic expression of the fit is:

$$\log\left(\frac{[\rm C\,II]}{\rm FIR}\right) = 1.21(\pm 0.24) - 0.35(\pm 0.03) \times \log(\Sigma_{\rm IR}) \quad (4)$$

with a dispersion in the y-axis of 0.15 dex. The slope and intercept of this trend are indistinguishable (within the uncertainties) from those obtained in Equation (3), which was derived by fitting all data-points including low 6.2 μm PAH EW sources with measured mid-IR sizes. This further supports the idea that the influence of AGN activity is negligible among IR-selected galaxies with $10^{-3} <$ [C II]/FIR $< 10^{-2}$ and that the increase in IR luminosity of these sources is due to a boost of their warm dust emission.

4.2.2. The Influence of AGNs in the [C II] Deficit

Figure 6 shows the [C II]157.7 μm/FIR ratio as a function of the 6.2 μm PAH EW for the LIRGs in GOALS. Starburst sources with large PAH EWs have a mean [C II]/FIR ratio of 4.0×10^{-3} with a standard deviation of 2.6×10^{-3}. As the 6.2 μm PAH EW becomes smaller the dispersion increases and we find galaxies with both very small ratios as well as sources with normal values (or slightly lower than those) typical of purely star-forming sources (see also Sargsyan et al. 2012).

If AGNs contribute significantly to the FIR emission of LIRGs and/or suppress PAH emission via photo-evaporation of its carriers, we would expect AGN-dominated sources to show significantly low [C II]/FIR ratios and small PAH EWs. We have used the *Spitzer*/IRS spectra of our galaxies to identify which of them are hosting an AGN based on several mid-IR diagnostics: (1) [Ne V]14.32 μm/[Ne II]12.81 μm $>$ 0.5; (2) [O IV]25.89 μm/[Ne II]12.81 μm $>$ 1; (3) S_{ν} 30 μm/S_{ν} 15 μm $<$ 6 (i.e., $\alpha > -2.6$ for $S_{\nu} \propto \nu^{\alpha}$); as well as (4) the 6.2 μm PAH EW itself (see constraints above). All these thresholds are rather restrictive and ensure that the contribution of an AGN to the mid-IR luminosity of a galaxy is *at least* 25%–50%. In Figure 6 we mark those sources that have at least two positive indicators of AGN activity as red stars. We note that this excludes sources with low 6.2 μm PAH EWs and no other AGN signatures, and is a more conservative cut than applied in Petric et al. (2011) to identify potential AGNs. Strikingly, these sources are not preferentially found at the bottom left of the parameter space but instead as many as 2/3 show [C II]/FIR $> 10^{-3}$, typical of star-forming sources with large 6.2 μm PAH EWs. This suggests that the impact of the AGN on the FIR luminosity of these mid-IR dominated AGN LIRGs is very limited, unless the it contributes to both the [C II] and FIR in the same relative amount as the starburst does.

While ∼18% of our sample appears to have significant AGN contribution to the mid-IR emission (Petric et al. 2011), the fraction in which the AGN dominates the bolometric luminosity of the galaxy is much smaller. To investigate this, we use two of the indicators described above, the [O IV]25.89 μm line and the 6.2 μm PAH EW, and the formulation given in Veilleux et al. (2009) to calculate the bolometric AGN fraction of those galaxies with at least two mid-IR AGN detections. We find that only four (20%) of these galaxies have contributions >50% in both indicators (black crosses in Figure 6). Two galaxies have [C II]/FIR $< 10^{-3}$ (33%) and two (14%) a larger ratio.

To quantitatively assess the relationship between AGN activity and the [C II]/FIR ratio among galaxies hosting an AGN, it is important to estimate first the AGN contribution to the FIR flux. If we assume that the ratio of [C II]157.7 μm to 6.2 μm PAH emission of the star-forming LIRGs in GOALS is constant, as is the case for most normal, lower luminosity galaxies (Helou et al. 2001; Croxall et al. 2012; Beirão et al. 2012), we can calculate the expected evolution of the [C II]/FIR ratio as a function of the 6.2 μm PAH EW if we also assume that pure starbursts have a typical 6.2 μm PAH $\rm EW_{SB} = 0.65$ μm and [C II]/FIR $= 4.0 \times 10^{-3}$ (as shown above), and that the average $L_{\rm FIR}/\nu L_{\nu\,6\,\mu{\rm m}}$ ratios for pure star-forming galaxies and AGNs are ∼15 and ∼1, respectively. The value for star-forming galaxies varies from ∼12–25 in our sample while the value for AGNs has been estimated from the intrinsic AGN spectral energy distribution of Mullaney et al. (2011). The predicted trend is shown in Figure 6 as a solid black line, which agrees very well with the location of the AGNs identified with at least two mid-IR indicators (red stars). Under these assumptions, the 6.2 μm PAH EW has to be reduced by a factor of ∼15 with respect to the 6.2 μm PAH $\rm EW_{SB}$, i.e., down to ≃0.05 μm, before the AGN can contribute 50% to the $L_{\rm FIR}$. In fact, 2/3 of galaxies with EWs lower than this threshold have been identified as harboring an AGN by two or more mid-IR diagnostics. Therefore, only when the AGN contribution to the FIR flux is significant do we see a noticeable decrease of the [C II]/FIR ratio (always $<10^{-3}$). We note

however that the contrary might not be necessarily true since there are galaxies with low [C II]/FIR ratios but with 6.2 μm PAH EWs $\gtrsim$ 0.5 μm.

We emphasize that this prediction does not account for possible destruction of PAH molecules due to the AGN. However, if the reduction of the PAH EW was entirely due to this effect, we would expect a linear correlation between the [C II]/FIR ratio and the 6.2 μm PAH EW, which is described by the dashed line in Figure 6. As we can see, the mid-IR AGN-dominated galaxies do not follow the predicted trend, suggesting that PAH destruction is not important in LIRGs with [C II]/FIR $\gtrsim 10^{-3}$ at least at the scales probed by *Herschel* and *Spitzer*, in agreement with the results obtained in Díaz-Santos et al. (2011).

Nearly half of galaxies with [C II]/FIR $< 10^{-3}$ and 6.2 μm PAH EW $< 0.05\,\mu$m have no other direct mid-IR diagnostic that reveals the presence of an AGN. Interestingly, all of them are among the outliers found in Figure 3, showing an excess in the $S_{9.7\,\mu m}$ with respect to their observed [C II]/FIR. We argued in Section 4.1.2 that these galaxies are probably hosting an extremely warm and compact source, optically and geometrically thick, not associated with the star-forming regions producing the bulk of the [C II] and FIR. The energy source of this component is unknown, though, since both an AGN or an ultra-compact H II region could generate such mid-IR signatures. However, the monochromatic νL_ν 63/15 μm ratios displayed by these objects are $\gtrsim$5 (see color-coding in Figure 6), significantly higher than the typically flat spectrum seen in QSOs and pure AGN sources (Elvis et al. 1994; Mullaney et al. 2011) in which the hot dust emission dominates the mid-IR wavelengths up to ~30–50 μm, with νL_ν = constant, and fading beyond. This adds evidence to the result obtained above that this type of deeply embedded objects only dominate the luminosity of the galaxy in the mid-IR.

Furthermore, we would like to emphasize that the fact that the source of this warm, compact emission does not produce the detected PAH or [C II] emissions rules out models where PAH obscuration is invoked to explain the low PAH EWs found in these sources, since their observed [C II] flux compared to that of the FIR is also very low, implying that it is not extinction but rather the fact that the PDR emission of the warmest dust component in these LIRGs is actually extremely limited.

5. IMPLICATIONS FOR INTERMEDIATE- AND HIGH-REDSHIFT GALAXY SURVEYS

At intermediate redshifts, $z \sim$ 1–3, it has been found that IR-luminous galaxies span a wide range in [C II]/FIR ratios: $\sim 10^{-2}$–$10^{-3.5}$ (Stacey et al. 2010). A surprising discovery came from the most luminous systems, and the fact that many of them show values of this ratio similar to those found in local, lower luminosity galaxies (e.g., Maiolino et al. 2009; Hailey-Dunsheath et al. 2010; Sturm et al. 2010; Stacey et al. 2010). These results, added to a number of recent findings obtained from the analysis of mid-IR dust features of star-forming galaxies using *Spitzer*/IRS spectroscopy (e.g., Pope et al. 2008; Murphy et al. 2009; Desai et al. 2009; Menéndez-Delmestre et al. 2009; Díaz-Santos et al. 2010, 2011; Rujopakarn et al. 2011; Stierwalt et al. 2013) are pointing toward an emerging picture in which the local counterparts of the dominant population of IR-bright galaxies at intermediate and high redshifts ($z > 1$) are not extremely dusty systems with similar IR luminosities (i.e., local ULIRGs) but rather galaxies with more modest SFRs, or $L_{\rm IR} \simeq 10^{10-12}\,L_\odot$ (starbursts and LIRGs). Therefore, since GOALS is a complete, flux-limited sample of 60 μm rest-frame selected LIRGs systems in the local universe covering an IR luminosity range from $\sim 10^{10}$ to $\sim 10^{12}\,L_\odot$, the empirical relations we find can be used to estimate what might be seen in similar surveys of intermediate- and high-redshift IR-luminous galaxies.

Recently, Elbaz et al. (2011) has found that the majority of star-forming galaxies, from the nearby universe and up to $z \sim 2$, follow a "main sequence" (MS) that is depicted by a specific SFR ($\rm SSFR_{MS}$) that increases with redshift. Galaxies in the MS are characterized by producing stars in a quiescent mode, with very low efficiencies ($L_{\rm IR}/M_{\rm gas} \lesssim 10\ L_\odot/M_\odot$) and extended over spatial scales of several kiloparsecs (Daddi et al. 2010; Magdis et al. 2012). On the other hand, galaxies with high SSFRs are currently experiencing a strong and very efficient, but short-lived (less than few hundred megayears) starburst event, some of them probably consequence of a major merge interaction. The SSFR of local galaxies is anti-correlated with their compactness as measured in the mid-IR, as well as from radio wavelengths (see also Murphy et al. 2013). Therefore, the trends of [C II]/FIR with $\rm FEE_{13.2\,\mu m}$, $\Sigma_{15\,\mu m}$, and $\Sigma_{\rm IR}$ found in Sections 4.1.3 and 4.2.1 tell us not only about the compactness of the starburst region but also about the main mode of star formation itself. Sources with high [C II]/FIR ratios should belong to the MS while galaxies with low ratios will likely be compact, starbursting sources.

Because >80%–90% of the UV and optical light of star-forming LIRGs and ULIRGs is reprocessed by dust into the IR wavelengths (Howell et al. 2010), the $L_{\rm IR}/M_\star$ ratio is equivalent to their SSFR since the SFR is directly proportional to the IR luminosity, with $\rm SFR_{IR}/L_{IR} = 1.72 \times 10^{-10}\,M_\odot\ yr^{-1}\,L_\odot{}^{-1}$ (as derived in Kennicutt 1998). Using Equation (13) from Elbaz et al. (2011) we calculate that the SSFR of MS galaxies in the local universe is $\rm SSFR_{MS} \simeq 0.09\,Gyr^{-1}$. However, this equation does not take into account the dependence of the $\rm SSFR_{MS}$ on the stellar mass of galaxies. Thus, we combine it with the SFR versus $M_\star$ correlation obtained from the Sloan Digital Sky Survey sample by Elbaz et al. (2007), using a power-law index of 0.8 for the dependence of the SFR on $M_\star$ (their Equation (5)) and after normalizing it by the $\rm SSFR_{MS}$ at $z = 0$. This joint equation assumes that the exponential dependence of the $\rm SFR_{MS}$ as a function of $M_\star$ does not vary with z, which is roughly the case at least up to $z \sim$ 2–3 (see, e.g., Karim et al. 2011). We have used this normalization factor to derive the excess of SSFR in our galaxies (also called "starburstiness:" $\rm SSFR/SSFR_{MS}$). If we define starbursting galaxies as those having a SSFR $> 3 \times$ $\rm SSFR_{MS}$, then ~68% of the galaxies in GOALS would be classified as such.

Figure 7 shows the [C II]/FIR ratio as a function of the integrated SSFR normalized to the representative $\rm SSFR_{MS}$ of galaxies at $z \sim 0$ for our LIRG sample. The stellar mass values are taken from Howell et al. (2010) and were derived directly either from the Two Micron All Sky Survey K-band or the 3.6 μm IRAC luminosities using the $M_\star/L$ conversions from Lacey et al. (2008). The solid line represents a fit to pure star-forming galaxies with 6.2 μm PAH EWs $\geqslant$ 0.5 μm. The Pearson's test yields $r = -0.65$ ($p_r = 0$), while the Kendall's test provides $\kappa = -0.47$. The correlation coefficient derived from the robust fit is -0.76. We note that the SFR and $M_\star$ plotted here represent integrated measurements of our galaxies while the [C II] and FIR values were obtained from a single PACS spaxel, probing an area of ~9.″4 × 9.″4, which at the median distance of our LIRGs is equal to a projected physical size of ~4 kpc on a side (similar to a 0.″5 beam at $z \sim 2$); an aperture big enough to contain most of the galaxies' emission.

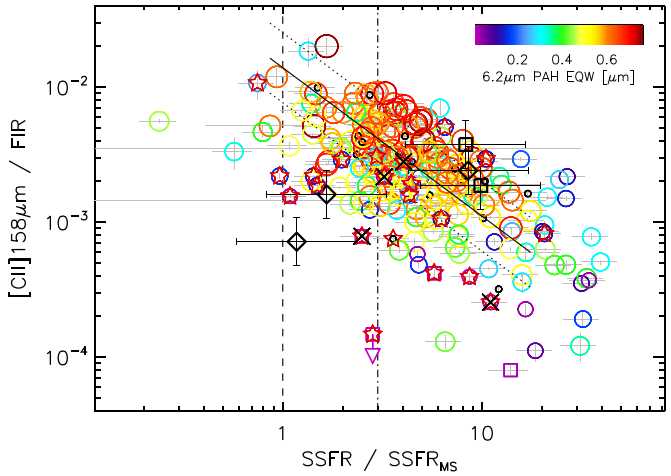

Figure 7. [C II]157.7 μm/FIR ratio vs. integrated SSFR normalized to the $\mathrm{SSFR_{MS}}(z \sim 0)$ for individual galaxies in the GOALS sample. Galaxies are color-coded as a function of their 6.2 μm PAH EW. Colored circles indicate sources for which an EW is available. Squares indicate lower limits. Small black circles are sources for which there is no information. The solid line is a fit to pure star-forming LIRGs only, excluding those sources that may harbor an AGN that could dominate their mid-IR emission (6.2 μm PAH EWs $<$ 0.5 μm; see Figure 6). The dotted lines are the $\pm 1\sigma$ uncertainty. The dashed line indicates the SSFR of MS galaxies at any redshift or $M_\star$. The dotted-dashed line represents $3 \times \mathrm{SSFR_{MS}}$, the limit above which galaxies are considered to be starbursting. The open squares represent two intermediate-redshift galaxies at $z \sim 1.2$, while the open diamonds represent three high-redshift sub-millimeter galaxies at $z \sim 4.5$ (see text for details).

(A color version of this figure is available in the online journal.)

In fact, if a 3×3 spaxel aperture is used instead, the fit yield virtually the same parameters as those reported below (within the uncertainties).

The trend between [C II]/FIR and normalized SSFR is not surprising since the IR luminosity appears in both quantities. Nevertheless, the correlation is indeed practical in terms of its predictive power. For example, we can see that there are no star-forming MS galaxies with [C II]/FIR $< 10^{-3}$. Their median ratio is 4.2×10^{-3}. On the other hand, starbursting sources show a larger range of ratios, from 10^{-2} to 10^{-4}, with a median of 1.9×10^{-3}. The correlation between the [C II]/FIR and the $\mathrm{SSFR/SSFR_{MS}}$ is given by the following equation:

$$\log\left(\frac{[\mathrm{C\,II}]}{\mathrm{FIR}}\right) = -1.86(\pm 0.03) - 1.09(\pm 0.07) \times \log\left(\frac{\mathrm{SSFR}}{\mathrm{SSFR_{MS}}}\right) \quad (5)$$

with a dispersion in the y-axis of 0.26 dex. If the separation between MS and starbursting galaxies (high/low [C II]/FIR) at any given redshift is related to an increase of the star formation efficiency (higher $L_{\mathrm{IR}}/M_{\mathrm{H_2}}$; see, e.g., Graciá-Carpio et al. 2011; Sargent et al. 2013) then this equation can be applied to predict the [C II] luminosity of star-forming galaxies at any z for which a measurement of the (far-)IR luminosity and stellar mass are available as long as their SSFR is normalized to the $\mathrm{SSFR_{MS}}$ at that z to account for the increase in gas mass fraction ($M_{\mathrm{gas}}/M_\star$) and therefore SSFR of MS galaxies at higher redshifts (Daddi et al. 2010; Magdis et al. 2012). Conversely, in future large IR surveys like those projected with the CCAT, this relation could be used for estimating the SSFR or stellar mass of detected galaxies when their [C II] and FIR luminosities are known.

As an example, in Figure 7 we show two intermediate-redshift $z \sim 1.2$ galaxies from (Stacey et al. 2010; SMMJ123633 and 3C368) and three high-redshift $z \sim 4.5$ sub-millimeter galaxies (SMGs; LESS 61.1 and LESS 65.1: Swinbank et al. 2012; LESS 033229.3: De Breuck et al. 2011; Wardlow et al. 2011) marked as open black squares and diamonds, respectively. To calculate the SFR of the SMGs we assumed that their $L_{\mathrm{IR}} \simeq 2 \times L_{\mathrm{FIR}}$. Since Equation (13) from Elbaz et al. (2011) is calibrated only up to $z \sim 3$ and the dependence of the $\mathrm{SSFR_{MS}}$ on $M_\star$ is also uncertain beyond this redshift, we normalized the SSFR of the SMGs by the $\mathrm{SSFR_{MS}}$ at $z = 3$. As we can see, three galaxies follow the correlation suggesting that they are starbursting sources with [C II]/FIR ratios consistent with their normalized SSFRs. On the other hand, the two remaining high-z SMGs show significantly lower [C II]/FIR ratios than the average of LIRGs for the same normalized SSFR. In particular, one of them display a [C II]/FIR more than an order of magnitude lower than the value predicted by the fit to our local galaxy sample. Interestingly, both SMGs lie in the parameter space where most of the mid-IR identified AGN are located (red stars). This may suggest that these two galaxies could harbor AGN or unusually week [C II] emission for their normalized SSFR.

Equations (3) and (4) can also be used to predict the mid- and total IR luminosity surface density of star-forming galaxies at high redshifts for which the [C II] and FIR fluxes are known, such as those that may be found in future spectroscopic surveys with the X-Spec instrument on CCAT. With instantaneous coverage over all the atmospheric windows between 190 and 440 GHz, X-Spec will access the [C II] line at redshifts from $\sim$3.5 to $\sim$9. Moreover, if a measurement of the rest-frame mid-IR luminosity of galaxies is also available, this correlation can be further used to estimate the physical size of the star-forming region in the mid-IR. This is particularly useful for $z \gtrsim 3$ sources detected with *Herschel* in deep fields. In these cases, the predicted mid-IR size of galaxies could be compared with direct measurements of the size of their FIR emitting region as observed with ALMA on physical scales similar to those we are probing in our GOALS LIRGs with PACS.

Table 2
Fraction of AGN

[C II]/FIR Range (1)	AGN-frac 6.2 μm PAH (2)	AGN-frac Multi (3)	63/158 μm Median (4)
$>5 \times 10^{-3}$	4%	2%	0.52
$(1.5\text{–}5) \times 10^{-3}$	15%	10%	0.93
$(0.5\text{–}1.5) \times 10^{-3}$	18%	9%	1.22
$<5 \times 10^{-4}$	72%	22%	1.92
63/158 μm Range (1)	**AGN-frac 6.2 μm PAH (2)**	**AGN-frac Multi (3)**	**[C II]/FIR Median (4)**
<0.5	8%	4%	7.0×10^{-3}
0.5–1	9%	8%	3.2×10^{-3}
1–2	28%	14%	1.5×10^{-3}
>2	56%	13%	5.8×10^{-4}

Notes. Top: Columns—(1) range of [C II]/FIR ratio; (2) percentage of mid-IR detected AGN based only on the 6.2 μm PAH EW of galaxies (<0.3 μm; see Section 4.2); (3) percentage of mid-IR detected AGN based on multiple line and continuum emission diagnostics (see text); (4) median S_ν 63 μm/S_ν 158 μm continuum flux density ratio within the range of [C II]/FIR given in Column 1. Bottom: Columns—(1) range of S_ν 63 μm/S_ν 158 μm continuum flux density ratio; (2) percentage of mid-IR detected AGN based only on the 6.2 μm PAH EW of galaxies (see text); (3) percentage of mid-IR detected AGN based on multiple line and continuum emission diagnostics (see text); (4) median [C II]/FIR ratio within the range of S_ν 63 μm/S_ν 158 μm given in Column 1.

Finally, because GOALS is a complete flux-limited sample of local LIRGs, we are able to predict the contamination of sources hosting AGNs in future large-scale surveys with both [C II] and FIR measurements. In Table 2 we provide the percentages of galaxies with mid-IR detected AGNs classified in different [C II]/FIR and S_ν 63 μm/S_ν 158 μm bins. The values provided in the table were computed using two conditions for the detection of the AGN that serve as upper and lower limits for the estimated fractions (Columns 2 and 3). The first was based on the 6.2 μm PAH EW only and the second required of an additional mid-IR diagnostic to classify the galaxy as harboring an AGN (see above). For example, we predict an AGN contamination (based on the 6.2 μm PAH EW only) of up to $\sim$70% for [C II]/FIR $< 5 \times 10^{-4}$, which implies that at least $\sim$1/3 of IR-selected sources with extremely low [C II]/FIR ratios will be powered by starbursts. Moreover, at the levels of [C II]/FIR $\geqslant 5 \times 10^{-4}$ or 63/158 μm < 2, the AGN detection fraction is expected to be $\lesssim$20%–25%.

6. CONCLUSIONS

We obtained new *Herschel*/PACS [C II]157.7 μm spectroscopy for 200 LIRG systems in GOALS, a 60 μm flux-limited sample of all LIRGs detected in the nearby universe. A total of 241 individual galaxies where observed in the [C II]157.7 μm line. We combined this information together with *Spitzer*/IRS spectroscopic data to provide the context in which the observed [C II] luminosities and [C II]/FIR ratios are best explained. We have found the following results.

1. The LIRGs in GOALS span two orders of magnitude in [C II]/FIR, from $\sim 10^{-2}$ to 10^{-4}, with a median of 2.8×10^{-3}. ULIRGs have a median of 6.3×10^{-4}. The $L_{[\mathrm{C\,II}]}$ range from $\sim 10^7$ to $2 \times 10^9\ L_\odot$ for the whole sample. The [C II]/FIR ratio is correlated with the FIR S_ν 63 μm/S_ν 158 μm continuum color. We find that all galaxies follow the same trend independently of their L_{IR}, suggesting that the main observable linked to the variation of the [C II]/FIR ratio is the average dust temperature of galaxies, which is driven by an increase of the ionization parameter, $\langle U \rangle$.
2. There is a clear trend for LIRGs with deeper 9.7 μm silicate strengths ($S_{9.7\,\mu\mathrm{m}}$), higher mid-IR luminosity surface densities (Σ_{MIR}), smaller fractions of extended emission ($\mathrm{FEE}_{13.2\,\mu\mathrm{m}}$) and higher SSFRs to display lower [C II]/FIR ratios. These correlations imply the dust responsible for the mid-IR absorption must be directly linked to the process driving the observed [C II] deficit. LIRGs with lower [C II]/FIR ratios are more warm and compact (higher mid- and IR luminosity surface densities, $\Sigma_{(\mathrm{M})\mathrm{IR}}$), regardless of what is the origin of the nuclear power source. However, this trend is clearly seen also among pure star-forming LIRGs only, implying that it is the compactness of the starburst, and not AGN activity as identified in the mid-IR, that is the main driver for the declining of the [C II] to FIR dust emission. This implies that the [C II] luminosity is *not* a good indicator of the SFR in LIRGs with high T_{dust} or large Σ_{IR} since it does not scale linearly with the warm dust emission most likely associated to the youngest stars. There are a small number of LIRGs that have a larger [C II]/FIR ratio than suggested by their deep $S_{9.7\,\mu\mathrm{m}}$ and warm dust emission. The origin of the energy source of these LIRGs is unknown, although they likely contain a deeply buried, compact source with little or no PDR emission.
3. Pure star-forming LIRGs (6.2 μm PAH EW $\geqslant 0.5$) have a mean [C II]/FIR $= 4.0 \times 10^{-3}$ with a standard deviation of 2.6×10^{-3}, while galaxies with low 6.2 μm PAH EWs span the entire range in [C II]/FIR. A significant fraction (70%) of the LIRGs in which an AGN is detected in the mid-IR have [C II]/FIR ratios $\geqslant 10^{-3}$, similar to those of starburst galaxies suggesting that most AGNs do not contribute substantially to the FIR emission. Thus, only in the most extreme cases when [C II]/FIR $< 10^{-3}$ might the AGN contribution be significant.
4. The completeness of the GOALS LIRG sample has allowed us to provide meaningful predictions about the [C II], Σ_{MIR}, and AGN contamination of large samples of IR-luminous high-redshift galaxies soon to be observed by ALMA or CCAT. In a FIR selected survey of high-z LIRGs we expect to find up to $\sim$70% of AGN contamination for [C II]/FIR $< 5 \times 10^{-4}$, which implies that at least 1/3 of IR-selected sources with extremely low [C II]/FIR will be powered by starbursts. Moreover, above this ratio the AGN fraction is expected to be $\lesssim$20%–25%. For deep fields with [C II] and FIR emission measurements we can predict the IR luminosity surface density of galaxies, which could be compared with direct measurements of the size of their FIR emitting region as observed with ALMA on physical scales similar to those we are probing in our GOALS LIRGs with PACS.

We thank the referee for useful comments and suggestions which significantly improved the quality of this paper. We also thank David Elbaz, Alexander Karim, J. D. Smith, Moshe Elitzur, and J. Graciá-Carpio for very fruitful discussions. L.A. acknowledges the hospitality of the Aspen Center for Physics, which is supported by the National Science Foundation Grant No. PHY-1066293. V.C. acknowledges partial support from the EU FP7 Grant PIRSES-GA-2012-31578. This work is based on observations made with the *Herschel Space Observatory*, an European Space Agency Cornerstone Mission with science instruments provided by European-led Principal Investigator consortia and significant participation from NASA. The *Spitzer Space Telescope* is operated by the Jet Propulsion Laboratory, California Institute of Technology, under NASA contract 1407. This research has made use of the NASA/IPAC Extragalactic Database (NED), which is operated by the Jet Propulsion Laboratory, California Institute of Technology, under contract with the National Aeronautics and Space Administration, and of NASA's Astrophysics Data System (ADS) abstract service.

APPENDIX

In Section 4.1.1, Figure 2, we show the [C II]157.7 μm/FIR ratio as a function of the PACS-based S_ν 63 μm/S_ν 158 μm ratio for the galaxies in the GOALS sample observed with *Herschel*, and explain the reasons for adopting and plotting this FIR color instead the more commonly used *IRAS*-based S_ν 60 μm/S_ν 100 μm color. Here we show a comparison between both, to provide the reader with a tool for interpreting our results in terms of *IRAS* colors, if necessary. Figure 8 shows that the FIR ratios correlate well ($r = 0.89$, $p_r = 0$), as expected, with a slope of 1.80 ± 0.08, an intercept of 0.30 ± 0.02, and a dispersion in the y-axis of 0.10 dex. We note that part of the scatter is caused by LIRG systems comprised by more than one galaxy, for which we have used their individual 63/158 μm ratios but the same 60/100 μm ratio, as they correspond to a single, unresolved *IRAS* source. Nevertheless, independently of

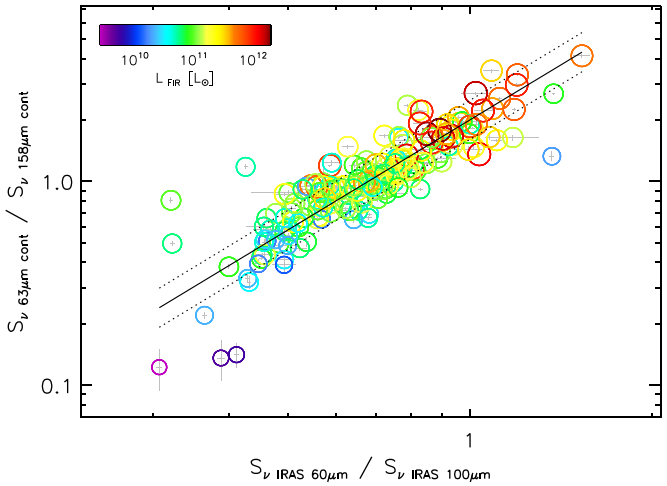

Figure 8. PACS-based S_ν 63 μm/S_ν 158 μm ratio as a function of *IRAS*-based S_ν 60 μm/S_ν 100 μm ratio for individual galaxies in the GOALS sample. In LIRG systems with two or more galaxies, the same *IRAS* color is plotted for each individual galaxy. The calculation of the $L_{\rm FIR}$ and the symbols are as in Figure 2.

(A color version of this figure is available in the online journal.)

which of these FIR colors we utilize, the same overall trend seen in Figure 2 emerges, namely warmer galaxies display smaller [C II]/FIR ratios. As mentioned in Section 4.1.1, when we use the *IRAS* FIR colors of integrated systems, our LIRG sample follows the same trend found for normal and moderate IR-luminous galaxies observed by *ISO*. However, when using the 63/158 μm ratio, the anti-correlation is tighter than that obtained when the emission from entire systems is employed, likely due to the fact that we are able to disentangle the true FIR colors of individual galaxies. Moreover, the observed 63/158 μm continuum ratios span a much larger dynamical range (a factor of ∼10, in contrast with the factor of ∼3 covered by the integrated 60/100 μm ratios), which translates in a more accurate sampling of the average dust temperature of LIRGs.

REFERENCES

Abel, N. P., Dudley, C., Fischer, J., Satyapal, S., & van Hoof, P. A. M. 2009, ApJ, 701, 1147
Alonso-Herrero, A., Pereira-Santaella, M., Rieke, G. H., & Rigopoulou, D. 2012, ApJ, 744, 2
Armus, L., Charmandaris, V., Bernard-Salas, J., et al. 2007, ApJ, 656, 148
Armus, L., Mazzarella, J. M., Evans, A. S., et al. 2009, PASP, 121, 559
Beirão, P., Armus, L., Helou, G., et al. 2012, ApJ, 751, 144
Berta, S., Magnelli, B., Nordon, R., et al. 2011, A&A, 532, A49
Brauher, J. R., Dale, D. A., & Helou, G. 2008, ApJS, 178, 280
Caputi, K. I., Lagache, G., Yan, L., et al. 2007, ApJ, 660, 97
Colbert, J. W., Malkan, M. A., Clegg, P. E., et al. 1999, ApJ, 511, 721
Contini, M. 2013, MNRAS, 429, 242
Croxall, K. V., Smith, J. D., Wolfire, M. G., et al. 2012, ApJ, 747, 81
da Cunha, E., Charmandaris, V., Díaz-Santos, T., et al. 2010, A&A, 523, A78
Daddi, E., Bournaud, F., Walter, F., et al. 2010, ApJ, 713, 686
De Breuck, C., Maiolino, R., Caselli, P., et al. 2011, A&A, 530, L8
Desai, V., Armus, L., Spoon, H. W. W., et al. 2007, ApJ, 669, 810
Desai, V., Soifer, B. T., Dey, A., et al. 2009, ApJ, 700, 1190
Díaz-Santos, T., Charmandaris, V., Armus, L., et al. 2010, ApJ, 723, 993
Díaz-Santos, T., Charmandaris, V., Armus, L., et al. 2011, ApJ, 741, 32
Draine, B. T. 1978, ApJS, 36, 595
Elbaz, D., Daddi, E., Le Borgne, D., et al. 2007, A&A, 468, 33
Elbaz, D., Dickinson, M., Hwang, H. S., et al. 2011, A&A, 533, A119
Elvis, M., Wilkes, B. J., McDowell, J. C., et al. 1994, ApJS, 95, 1
Fischer, J., Sturm, E., González-Alfonso, E., et al. 2010, A&A, 518, L41
Genzel, R., Lutz, D., Sturm, E., et al. 1998, ApJ, 498, 579
González-Alfonso, E., Smith, H. A., Fischer, J., & Cernicharo, J. 2004, ApJ, 613, 247
González-Martín, O., Rodríguez-Espinosa, J. M., Díaz-Santos, T., et al. 2013, A&A, 553, A35
Goulding, A. D., Alexander, D. M., Bauer, F. E., et al. 2012, ApJ, 755, 5
Graciá-Carpio, J., Sturm, E., Hailey-Dunsheath, S., et al. 2011, ApJL, 728, L7
Haan, S., Surace, J. A., Armus, L., et al. 2011, AJ, 141, 100
Habing, H. J. 1968, BAN, 19, 421
Hailey-Dunsheath, S., Nikola, T., Stacey, G. J., et al. 2010, ApJL, 714, L162
Hayes, M. A., & Nussbaumer, H. 1984, A&A, 134, 193
Helou, G., Khan, I. R., Malek, L., & Boehmer, L. 1988, ApJS, 68, 151
Helou, G., Malhotra, S., Hollenbach, D. J., Dale, D. A., & Contursi, A. 2001, ApJL, 548, L73
Howell, J. H., Armus, L., Mazzarella, J. M., et al. 2010, ApJ, 715, 572
Inami, H., Armus, L., Charmandaris, B., et al. 2013, ApJ, submitted
Iwasawa, K., Sanders, D. B., Teng, S. H., et al. 2011, A&A, 529, A106
Karim, A., Schinnerer, E., Martínez-Sansigre, A., et al. 2011, ApJ, 730, 61
Kaufman, M. J., Wolfire, M. G., Hollenbach, D. J., & Luhman, M. L. 1999, ApJ, 527, 795
Kennicutt, R. C., Jr. 1998, ApJ, 498, 541
Kim, D.-C., Evans, A. S., Vavilkin, T., et al. 2013, ApJ, 768, 102
Lacey, C. G., Baugh, C. M., Frenk, C. S., et al. 2008, MNRAS, 385, 1155
Laurent, O., Mirabel, I. F., Charmandaris, V., et al. 2000, A&A, 359, 887
Levenson, N. A., Sirocky, M. M., Hao, L., et al. 2007, ApJL, 654, L45
Luhman, M. L., Satyapal, S., Fischer, J., et al. 1998, ApJL, 504, L11
Magdis, G. E., Daddi, E., Bthermin, M., et al. 2012, ApJ, 760, 6
Magnelli, B., Elbaz, D., Chary, R. R., et al. 2011, A&A, 528, A35
Maiolino, R., Caselli, P., Nagao, T., et al. 2009, A&A, 500, L1
Malhotra, S., Helou, G., Stacey, G., et al. 1997, ApJL, 491, L27
Malhotra, S., Kaufman, M. J., Hollenbach, D., et al. 2001, ApJ, 561, 766
Menéndez-Delmestre, K., Blain, A. W., Smail, I., et al. 2009, ApJ, 699, 667
Mullaney, J. R., Alexander, D. M., Goulding, A. D., & Hickox, R. C. 2011, MNRAS, 414, 1082
Murphy, E. J., Chary, R., Alexander, D. M., et al. 2009, ApJ, 698, 1380
Murphy, E. J., Chary, R.-R., Dickinson, M., et al. 2011, ApJ, 732, 126
Murphy, E. J., Stierwalt, S., Armus, L., Condon, J. J., & Evans, A. S. 2013, ApJ, 768, 2
Negishi, T., Onaka, T., Chan, K.-W., & Roellig, T. L. 2001, A&A, 375, 566
Nenkova, M., Sirocky, M. M., Nikutta, R., Ivezić, Ž., & Elitzur, M. 2008, ApJ, 685, 160
Nikola, T., Genzel, R., Herrmann, F., et al. 1998, ApJ, 504, 749
Paladini, R., Umana, G., Veneziani, M., et al. 2012, ApJ, 760, 149
Petric, A. O., Armus, L., Howell, J., et al. 2011, ApJ, 730, 28
Pilbratt, G. L., Riedinger, J. R., Passvogel, T., et al. 2010, A&A, 518, L1
Poglitsch, A., Waelkens, C., Geis, N., et al. 2010, A&A, 518, L2
Pope, A., Chary, R.-R., Alexander, D. M., et al. 2008, ApJ, 675, 1171
Rujopakarn, W., Rieke, G. H., Eisenstein, D. J., & Juneau, S. 2011, ApJ, 726, 93
Sanders, D. B., Mazzarella, J. M., Kim, D.-C., Surace, J. A., & Soifer, B. T. 2003, AJ, 126, 1607
Sanders, D. B., & Mirabel, I. F. 1996, ARA&A, 34, 749
Sargent, M. T., Daddi, E., Béthermin, M., et al. 2013, arXiv:1303.4392
Sargsyan, L., Lebouteiller, V., Weedman, D., et al. 2012, ApJ, 755, 171
Siebenmorgen, R., Krügel, E., & Spoon, H. W. W. 2004, A&A, 414, 123
Sirocky, M. M., Levenson, N. A., Elitzur, M., Spoon, H. W. W., & Armus, L. 2008, ApJ, 678, 729
Spoon, H. W. W., Marshall, J. A., Houck, J. R., et al. 2007, ApJL, 654, L49
Stacey, G. J., Geis, N., Genzel, R., et al. 1991, ApJ, 373, 423
Stacey, G. J., Hailey-Dunsheath, S., Ferkinhoff, C., et al. 2010, ApJ, 724, 957
Stierwalt, S., Armus, L., Surace, J. A., et al. 2013, ApJS, 206, 1
Sturm, E., Verma, A., Graciá-Carpio, J., et al. 2010, A&A, 518, L36
Swinbank, A. M., Karim, A., Smail, I., et al. 2012, MNRAS, 427, 1066
Tielens, A. G. G. M., & Hollenbach, D. 1985, ApJ, 291, 722
Veilleux, S., Kim, D.-C., Sanders, D. B., Mazzarella, J. M., & Soifer, B. T. 1995, ApJS, 98, 171
Veilleux, S., Rupke, D. S. N., Kim, D.-C., et al. 2009, ApJS, 182, 628
Voit, G. M. 1992, MNRAS, 258, 841
Wang, Z., & Helou, G. 1992, ApJL, 398, L33
Wardlow, J. L., Smail, I., Coppin, K. E. K., et al. 2011, MNRAS, 415, 1479
Watson, W. D. 1972, ApJ, 176, 103
Wolfire, M. G., Hollenbach, D., McKee, C. F., Tielens, A. G. G. M., & Bakes, E. L. O. 1995, ApJ, 443, 152
Wolfire, M. G., Tielens, A. G. G. M., & Hollenbach, D. 1990, ApJ, 358, 116